Homogeneous nucleation rates of supercooled water measured in single levitated microdroplets

B. Krämer, O. Hübner, H. Vortisch, L. Wöste, and T. Leisner[a)]
Institut für Experimentalphysik, Freie Universität Berlin, Arnimallee 14, 14195 Berlin, Germany

M. Schwell,[b)] E. Rühl, [c)] and H. Baumgärtel
Institut für Physikalische und Theoretische Chemie, Freie Universität Berlin, Takustr. 3, 14195 Berlin, Germany

(Received 25 May 1999; accepted 20 July 1999)

Homogeneous nucleation rates are determined for micrometer sized water droplets levitated inside an electrodynamic Paul-trap. The size of a single droplet is continuously measured by analyzing the angle-resolved light scattering pattern of the droplets with classical Mie theory. The freezing process is detected by a pronounced increase in the depolarization of the scattered light. By statistical analysis of the freezing process of some thousand individual droplets, we obtained the homogeneous nucleation rate of water between 236 and 237 K. The values are in agreement with former expansion cloud chamber measurements but could be determined with considerably higher precision. The measurements are discussed in the light of classical nucleation theory in order to obtain the size and the formation energy of the critical nucleus. © *1999 American Institute of Physics.* [S0021-9606(99)02738-5]

INTRODUCTION

Droplets of supercooled water are known to exist in the stratosphere and the upper troposphere.[1,2] Here homogeneous ice nucleation is the controlling mechanism for the formation of cirrus clouds and thereby affects directly the radiation balance of the earth.

The phase equilibria of the water–ice system are very well known and documented by reliable data. The theoretical description based on thermodynamics is fully developed. The situation is different for the rate of homogeneous phase transitions however. It is generally accepted that the phase transition follows a nucleation-growth mechanism as described by the classical nucleation theory.[3–11] According to this theory the phase transition is initiated by the formation of nuclei of the solid phase in the liquid phase. These nuclei need a critical size in order to grow further and complete the phase transition. The nucleation rate describes the probability that such a single nucleus of critical size is formed per unit time and unit volume. Despite its importance for the kinetics of phase transitions, only a few experimental data are available. For substances which feature directed intermolecular bonds it is still not possible to calculate nucleation rates *ab initio*. In the case of supercooled water the structure is still discussed in the frame of different models.[11–18]

Nucleation rates in supercooled water have been measured by several groups based on experiments in cloud chambers,[19–22] on supercooled water droplets in hydrophobic media[23] and by field measurements.[24–26] Using reasonable experimental input data the nucleation rates have been calculated using the classical nucleation theory.[27,28] The experimental values and the calculated values are consistent, but only within large error limits.

This situation was the reason to establish an improved experiment[29] to measure homogeneous nucleation rates in single droplets of supercooled water at temperatures around −37 °C. In our experiment we observe single droplets which are stored in an electrodynamic trap and are stationary in space for a long time. This technique can be traced back to Paul[30] and Wuerker[31] and has since then been widely used for aerosol studies. For a historical survey and more details see a recent review[32] and the references therein. The method offers three distinct advantages: The volume of each of the droplets can be determined with high precision. Additionally, there are no influences of the walls of a vessel and, therefore, any influence of heterogeneous nucleation can be excluded. Finally the time the droplet stays supercooled before the nucleation takes place can be measured with high accuracy.

The present work extends earlier and preliminary work on homogeneous nucleation of supercooled water.[27] Systematic studies are presented in order to derive reliable results on homogeneous nucleation rates, the influence of electrical charges to the nucleation process, size effects in homogeneous nucleation, estimates of the critical nucleus, as well as the analysis of the polarization properties of the elastically scattered light of frozen ice particles, that can be compared to remote sensing experiments on atmospheric aerosols.

EXPERIMENT

Our measurements of the homogeneous nucleation rate of water were carried out using single weakly charged microdroplets of water which were levitated under a controlled

[a)]Author to whom correspondence should be addressed. Electronic mail: leisner@physik.fu-berlin.de
[b)]Present address: Université de Cergy-Pontoise Neuville F-95031 Cergy-Pontoise Cedex, France.
[c)]Present address: Fachbereich Physik, Universität Osnabrück, Barbarastr. 7, D-49069 Osnabrück, Germany.

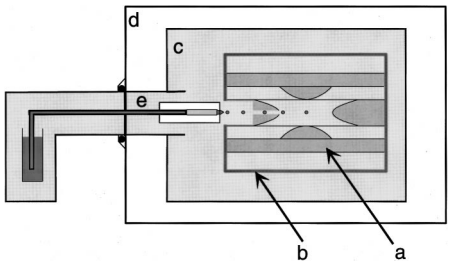

FIG. 1. Schematic view of the experimental setup. (a) Paul trap, (b) copper enclosure for thermal stability, (c) cooled climate chamber, (d) insulation vacuum chamber, and (e) heated droplet injector.

atmosphere in an electrodynamic trap. The liquid solid phase transition was detected by analyzing the scattered light from a He–Ne laser. This approach avoids any wall contact of the droplets and allows a precise size determination of the droplets, crucial prerequisites for the measurement of accurate nucleation rates. As homogeneous nucleation is a statistical process, it is necessary to observe a large number of single freezing events. Therefore we developed a trap setup which allows the controlled injection of single microdroplets into the trap while the trap chamber and its atmosphere reside on the low temperature of interest.[29] This approach is different from previous experiments where the freezing of supercooled trapped droplets was observed,[33,34] and therefore, we describe the experimental setup in some detail.

An overview of the apparatus is given in Fig. 1. It consists of the trap assembly [Figs. 1(a) and 1(b)], which is housed inside a climate chamber [Fig. 1(c)] which is surrounded by a controlled atmosphere with a pressure of about 1 bar and kept at the temperature of interest. This chamber is mounted inside a larger vacuum vessel [Fig. 1(d)] for thermal insulation. A total of eight ports allows for the insertion of the droplet injector [Fig. 1(e)], the laser beam, and various diagnostic tools.

The droplets are levitated in a standard hyperboloidal electrodynamic levitator, which consists of a central ring electrode with bottom and top endcap electrodes. The central electrode carries the ac (alternating current) voltage for trapping, while the endcap electrodes are used to form an additional dc (direct current) field to balance the gravitational force on the droplets. All three electrodes have hyperboloidal shapes as required for a pure quadrupolar electric potential distribution inside the trap. The inner radius of the ring electrode is 5 mm and all the other dimensions are given by the requirement of a quadrupolar electric field. The torus electrode and the endcaps have 2 mm diam. holes for the injection of the droplets, for the laser beam, and the detection of the scattered light. The trap is tightly enclosed inside a copper chamber which carries the same ports and ensures a homogeneous temperature profile across the trap. It also minimizes atmospheric turbulences which might arise from a nonuniform cooling of the surrounding climate chamber. The climate chamber is sealed with metal gaskets and carries various view ports and electrical and gas feedthroughs. Its temperature is variable between 150 K and room temperature and is adjusted by means of liquid nitrogen cooling and resistive heating.

The temperature of the gas atmosphere in the trap is monitored by a platinum resistor located at one endcap electrode. Two additional thermocouples are placed at the top and the bottom of the copper enclosure. All temperature sensors are calibrated with ice–water and dry ice–acetone mixtures. The platinum resistor has a absolute precision of ± 0.2 K and can resolve temperature differences down to 50 mK. It is used to control and stabilize the temperature inside the trap. Due to the regulation mechanism during the experiment, only very slow temperature variations (± 0.3 K, within one hour) around the preset value are observed. Temperature differences at two points inside the trap chamber are less than ± 0.5 K, which is the resolution of the thermocouples.

The climate chamber is mounted inside the insulation chamber which is pumped by a turbomolecular pump and carries a quadrupole residual gas analyzer. It is used to monitor the composition of the atmosphere of the trap chamber, which is leaking from a 20 μm diam. pinhole into the insulation vacuum chamber.

Liquid water droplets in the diameter range from 10 to 70 μm are generated by piezo driven nozzles. Such generators can be triggered to produce single droplets of reproducible size, charge and velocity. They have been described previously[35] and are commercially available.[36] In order to span a large range of droplet sizes, we use home built devices however. The injector is mounted in close proximity to the toroidal ac electrode but outside the copper enclosure of the trap. As the droplet generators have to be operated above the freezing point of the liquid of interest, special care had to be taken to heat the nozzle and the liquid tubing, and to insulate it thermally from the cold atmosphere inside the trap chamber. The droplets are charged by induction from the ac voltage of the trap. During the experiment the nozzle is placed close to the ring electrode of the trap. The amount of charge on the droplet depends on the amplitude of the ac voltage on the ring electrode at the instant of injection. When the droplet breaks from the liquid filament, a majority of ions of one polarity resides on the droplet due to the attraction from the trap electrode potential. By varying the time of injection relative to the phase of the ac voltage, positively or negatively charged droplets which carry between zero and 10^7 elementary charges can be produced. If the correct moment of injection and the right ac amplitude and frequency are chosen, every single droplet can be stored inside the trap. Those droplets then carry between 10^6 and 10^7 elementary charges of either polarity.

The gravitational force on the droplet is balanced by a dc potential applied between the bottom and top electrode. The central position of the droplet inside the trap is maintained by a feedback loop. For this purpose, the droplet is imaged by an objective lens ($\times 10$ magnification) onto a linear CCD (charge coupled device) array detector. Its position is determined and stabilized by means of a home built electronic circuit that controls the dc voltage between bottom and top electrode. The required voltage reflects faithfully any changes in the mass to charge ratio of the droplets that might occur by evaporation or gas uptake. It is continuously read by a computer which is used to calculate and set the ideal values for the amplitude and frequency of the ac trapping

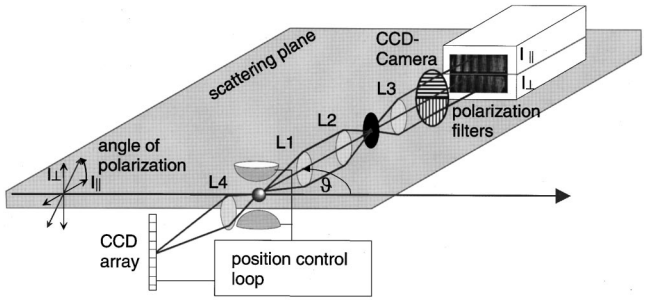

FIG. 2. Schematic view of the light scattering geometry and the optical setup. The ring electrode of the trap is omitted for clarity.

voltage. Thus, a constant trapping force is ensured even if the droplet mass changes by a factor of 10^5 due to evaporation. A scheme of this feedback loop is indicated in Fig. 2.

In order to determine the size and phase of the droplets, we analyze the angular distribution of the light scattered by the droplet from a He–Ne laser beam.[37] As shown in Fig. 2, the scattered light is imaged onto a CCD camera (512 $\times$784 pixel) which is positioned under an angle of 90° with respect to the laser beam. It has a total acceptance angle of 22.6° with an angular resolution of 0.03°. A first objective first lens (L1 in Fig. 2) collects the scattered light and forms it to an parallel beam. After passing the two windows of the climate and insulation chamber, the light passes a space filter consisting of two lenses (L2 and L3) and an aperture placed in between. In order to measure both polarization planes of the scattered light, two polarization filters are placed in front of the camera so that the perpendicular polarized component of the scattered light falls on the upper half and parallel polarized light on the lower half of the CCD sensor. Figure 3 shows a typical scattering image from a droplet which was illuminated with an laser beam which was polarized under 45° with respect to the scattering plane. Both polarization components show a distinct number of bright and dark stripes. The number of stripes is roughly proportional to the radius of the droplet.[38] To evaluate the radius and the index of refraction with higher precision, the angular distribution of intensity is compared to Mie-theory.[39] In this way, the index of refraction and the radius can be evaluated for droplets with a radius between 10 and 50 μm with an accuracy of $\pm$50 nm. A comparison between measured and calculated intensity distributions is shown in Fig. 4. The determination of both parameters can be repeated every 40 ms, at the rate pictures are taken with the CCD camera. Thus the evaporation velocity of a droplet can be evaluated.

In order to minimize possible effects of heterogeneous nucleation,[40] triply distilled water has been filtered through a 0.2 μm pore-size teflon membrane filter (Roth) and placed in the reservoir of the injection system. For cleaning the injector, 25 ml of the purified water is flushed through the system. The climate chamber is cooled down to the desired temperature (around 236 K for this experiment). A nitrogen atmosphere of 1 bar pressure is used. The heating system of the injector is switched on and the injector is placed inside the climate chamber. After 30 minutes the temperature inside the trap is equilibrated. Single droplets are then injected into the trap. They are produced at room temperature but thermalize

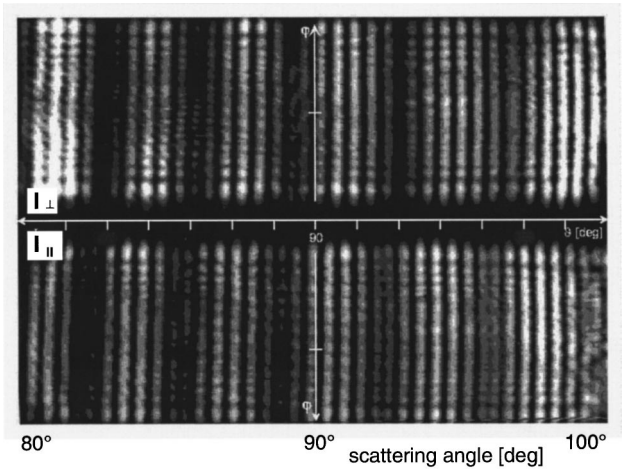

FIG. 3. Scattering pattern of a water droplet ($r=x.y$ μm) polarized perpendicular (top panel) and parallel (bottom panel) with respect to the scattering plane. The illuminating laser was polarized under 45°.

rapidly within the cold atmosphere of the trap. The time constant for thermalization depends strongly on the droplet size and can be calculated to be about 60 ms for droplets of 30 μm diam. For each droplet we measure the time until freezing occurs. For this purpose the droplet is illuminated with light polarized parallel to the scattering plane. Figure 5(a) shows the scattering pattern obtained from a liquid droplet. Since a spherical droplet does not change the plane of polarization, no perpendicular polarized light is detected. The scattering pattern shown in Fig. 5(b) corresponds to a frozen droplet. The stripes become irregular and intensity is found in the perpendicular polarization channel. The appearance of perpendicularly polarized light is used to evaluate the time after which freezing starts. As shown in Fig. 6, the parallel polarized light intensity grows at the time a droplet is injected (t_a). When the particle freezes intensity in the perpendicular light channel is observed (t_b). Between (t_a) and (t_b) the droplet stays supercooled. This time represents the nucleation time t_1. Finally, at time (t_c) the droplet is

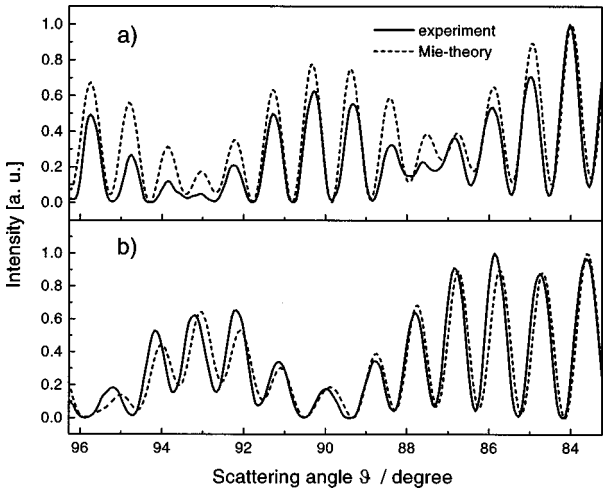

FIG. 4. Experimental and calculated angular distribution of the scattered light as used for the determination of size and refractive index of a spherical water droplet.

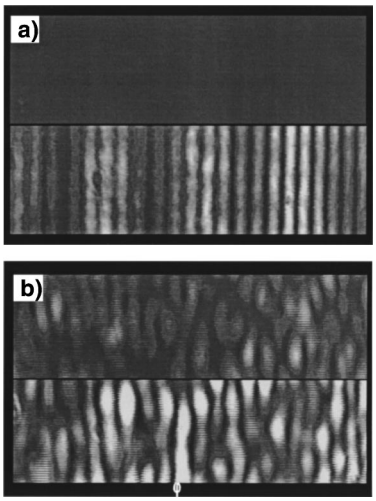

FIG. 5. Scattering pattern of (a) a liquid and (b) a frozen droplet illuminated by laser light polarized parallel to the scattering plane. The upper and lower panels correspond to perpendicular and parallel polarization of the scattered light, respectively.

ejected. This experiment is repeated at constant temperature for many droplets.

The process of homogeneous nucleation can be described by Poisson statistics,[41] since the probability for the formation of a nucleus at a certain time in a certain volume element of the droplet is assumed to be independent of the position of the volume element inside the droplet and the time of freezing. Integrating this statistical law in the limits of many observed events, we arrive at Eq. (1)

$$\ln(N_u(t)/N_0) = -J(T)\cdot V_d \cdot t. \tag{1}$$

$N_u(t)$ is the number of unfrozen droplets after time t, N_0 is the total number of investigated droplets, V_d is the volume of the droplet and $J(T)$ is the temperature dependent nucleation rate.

Figure 7 shows a typical plot of $\ln N_u/N_0$ against the nucleation time of the supercooled droplet. 200 droplets with a diameter of about 60 μm were investigated at 236.5 K. The

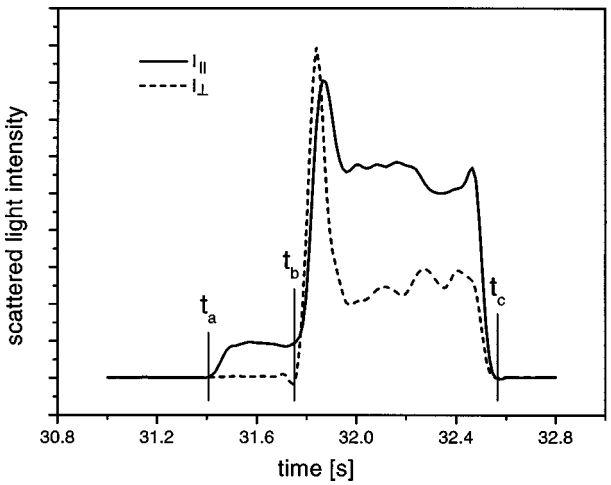

FIG. 6. Intensity of the light scattered from a parallel polarized laser beam into an angular range between 80° and 100° as a function of time and polarization. The following important times are marked: t_a moment of droplet injection t_b time of freezing t_c time of droplet ejection.

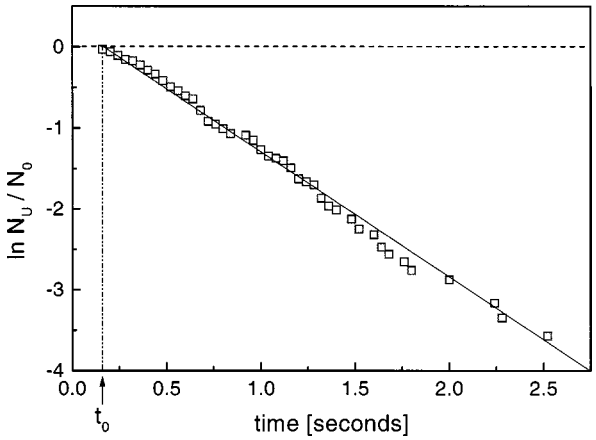

FIG. 7. Ratio of unfrozen droplets as a function of time after injection into the cold trap at 236 K. The slope of the linear fitting curve (straight line) is used to calculate the nucleation rate.

fit to the straight line confirms the good agreement of the homogeneous nucleation process with the statistical law discussed above. From the slope of this curve one can directly calculate the rate of homogeneous nucleation once the volume of the droplet is known. Only for a few droplets the size was determined directly by the evaluation of the light scattering as discussed above in order to confirm that the radius of the droplets as produced from the nozzle varies by only 0.5%. However, by careful analysis of the volume of every single droplet from the recorded light scattering data, the uncertainty of the measured nucleation rates shown below could further be reduced. The straight line in Fig. 7 intersects the $N_u/N_0=1$ line not at time zero, but at $t=0.16$ s. This is due to the finite time that is required to cool the droplets from the temperature of the injector ($\sim$283 K) down to the temperature of the trap ($\sim$236 K for water nucleation measurements). This time is, therefore, obtained separately from our measurements and does not influence the evaluation of the nucleation rate.

Long time observation of the droplets inside the trap is complicated by a steady evaporation of the droplets even at low temperature. The evaporation rate of a water droplet during the measurements depends on the content of water in the surrounding gas. In our experiment this is given by the vapor pressure of water above the ice on the walls of the climate chamber (about 100 ppm at 236 K). From the light scattering measurements the change of the radius was determined to be nearly constant throughout the experiment and amounts to 0.7 mm/s. The trapped liquid droplet stays—even during evaporation—in good thermal equilibrium with the surrounding gas atmosphere. This can be rationalized by the application of the laws of heat diffusion to a water droplet of 60 μm diam in a nitrogen atmosphere of 1 bar. Here evaporation at the observed rate cools the droplet to only 0.1 K below the temperature of the surrounding atmosphere.

Since the droplet is evaporating during the observation time, we have investigated only temperatures which lead to nucleation times less than 5 s. Thus, the measurable nucleation rate for droplets of 60 mm diam is thus limited to be above $10^7\,\mathrm{cm}^{-3}\,\mathrm{s}^{-1}$. The upper limit for the nucleation rate of $5\cdot 10^8\,\mathrm{cm}^{-3}\,\mathrm{s}^{-1}$ is given by the time necessary to cool the

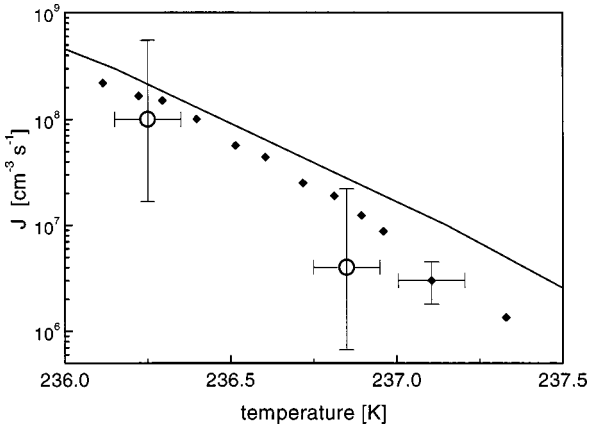

FIG. 8. Comparison of the nucleation rates measured in this experiment (filled diamonds) with values reported in Ref. 22 (open circles) and the curve calculated by Pruppacher (Ref. 27) using the improved classical nucleation theory.

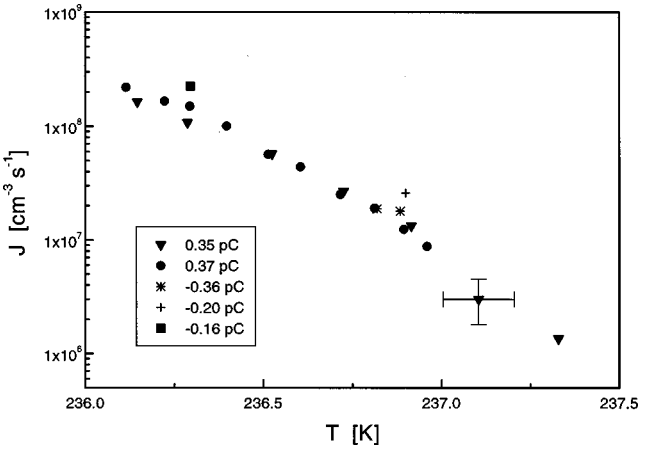

FIG. 9. Temperature dependence of the nucleation rate of water droplets carrying different charges.

droplet down to the ambient temperature in the climate chamber. For measuring a wider range of nucleation rates droplets of a different size will be investigated in the future.

RESULTS

We have observed the freezing of more than 2000 single water droplets in order to derive the homogeneous nucleation rate in a temperature interval between 236 and 237 K. The droplets all had a diameter of $60(\pm 2)$ μm and carried a charge of $36(\pm 2)$ pC. Figure 8 displays the obtained nucleation rates together with theoretical results reported by Pruppacher[27] and with results of DeMott and Rogers[22] from recent experiments in a cloud chamber. Each of the data points corresponds to a observation of several hundred droplets at constant temperature. The temperature dependent nucleation rates were then determined by fitting a straight line to the $\ln(N_u/N_0)$ versus t_1 plots as shown in Fig. 7. As can be seen from Fig. 8 the nucleation rate is strongly temperature dependent. Cooling by only one Kelvin leads to an increase of the nucleation rate by a factor of 70, as expected from the improved nucleation theory.[27] Our measurements follow in general the same temperature dependence as given by Pruppacher but are systematically lower by about a factor of two over most of the accessible range of nucleation rates. This is considerably less then in previous experiments.[22,27] It has to be noted, that the theoretical curve was not obtained from first principles but the diffusion activation energy of liquid water was fitted to the then available experimental data which had a much larger uncertainty, as discussed in detail below. Our results are consistent with the previous experiments within their large limits of error.

Since all droplets in our experiment have to be charged, we also investigated droplets of various charge states between -0.36 and $+0.37$ pC with a minimum of the absolute value of the charge at 0.16 pC. The results are given in Fig. 9. Taking the error limit into account, no influence of the charge on the nucleation rate could be found. Furthermore, the experiments verified that the measured nucleation rates do not depend on the size of the droplets in a diameter range between 30 and 60 μm.

As mentioned above, the frozen droplets depolarize the incident parallel polarized light. A measure for this is the depolarization ratio which is commonly defined as

$$\delta = I_\perp / I_\parallel , \tag{2}$$

where $I_\perp$ and $I_\parallel$ are the intensities of the perpendicular and parallel component of the scattered light, respectively. The depolarization ratio is often used to identify the physical phase of cloud droplets with *in situ* measurement techniques like LIDAR (light detecting and ranging).[42] Nevertheless for polycrystalline particles its absolute value cannot be easily accessed theoretically. In order to facilitate an empirical correlation between droplet properties and the depolarization ratio we have recorded the depolarization ratio of the frozen water droplets in our experiment by comparing the total scattered light intensity in both polarization channels. The intensities are averaged over the observation time and corrected for background light and errors occurring due to the use of polarization filters. Figure 10 shows an analysis of the depolarization ratio of 500 frozen water droplets. Most of the frozen particles have a depolarization ratio ranging between 0.1 and 0.5 with an average value of 0.39 and a full width at half maximum of ± 0.2. The maximum of the distribution is found for a depolarization ratio of 0.3. A depolarization ratio of 0.3 has also been found previously in high altitude cirrus clouds.[43] The width of the distribution reflects the variety of different scattering images from frozen water droplets. The product of the freezing process seems to be a polycrystalline frozen water droplet which exhibits a depolarization ratio depending on the distribution of the micro crystals inside the particle.

It is instructive to examine the observed scattering patterns of the frozen droplets in more detail. Figure 11 shows different scattering pictures of frozen water droplets. The incoming laser beam in this case was polarized under 45° with respect to the scattering plane. Many droplets show in the first moment after freezing a short peak in the intensity of the scattered light (cf. Fig. 6) accompanied by a scattering picture without structure as shown in Fig. 11(d). In some instances, the droplet even disintegrates during the crystallization process leaving behind one or two daughter particles.

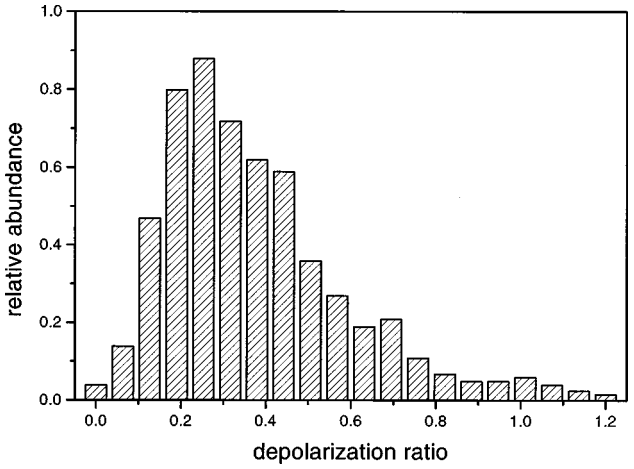

FIG. 10. Relative distribution of the depolarization ratios in frozen water droplets.

In the other cases, the scattering pattern becomes more structured after a few seconds. As shown in Fig. 11(a), sometimes a hexagonal structure is visible that might correspond to the hexagonal shape of ice crystals. This pattern is reproducible and was not observed with sulfuric acid solutions but only for pure water droplets. In most cases the scattered light shows a structure which is irregularly modulated on various scales [Figs. 11(b) and 11(c)]. Usually the scattering pattern becomes more regular after longer times. Therefore, we conclude that the droplet becomes a polycrystalline solid which remains more or less in a spherical shape after the phase change. Strong deviations from the spherical shape are probably smoothed out after some time due to evaporation and condensation processes which tend to minimize the surface area.

DISCUSSION

The homogeneous nucleation rates of supercooled water in a temperature interval from 236.1 to 237.3 K were measured with high precision. Our results confirm the classical picture of homogeneous nucleation.

The observed temperature dependence of the nucleation rate follows, but lies systematically somewhat below the curve given by Pruppacher.[27] We assume that this deviation is not related to the charge of the droplets, as we observe a nucleation rate that is within the limits of error independent of the size and charge of the droplets. This indicates that the freezing process starts by homogeneous nucleation in the volume phase of the droplet and not in the surface layer where the charges are located.

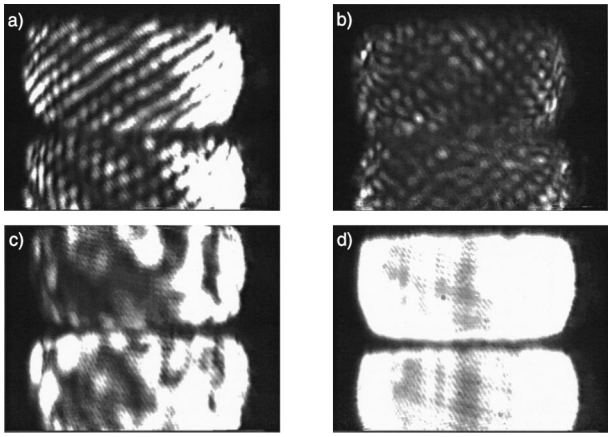

FIG. 11. (a)–(d) Different scattering patterns of frozen water droplets (see text). The upper and lower panels in each figure correspond to perpendicular and parallel polarization of the scattered light, respectively.

With respect to (Ref. 27), it should be noted that former applications of the classical theory of homogeneous nucleation of ice in water resulted in nucleation rates which were five orders of magnitude lower than the experimental values. According to Pruppacher,[27] this discrepancy has been caused by the derivation and extrapolation of the activation energy ΔF_{act} from experiments on selfdiffusion and viscosity of water at much higher temperatures. Therefore, and because results from alternative experimental approaches are not available, Pruppacher adjusted the temperature dependent activation energy in a way that the resulting nucleation rates fit the averaged results of the then known experiments which had a comparatively large error range. It is, therefore, not surprising that our measurements deviate systematically from this curve, but lie well within the error limits of the previous data on which the theory was based.

From the measured nucleation rate, the formation energy of the nucleus can be calculated according to a fundamental equation of the classical nucleation theory

$$J(T)=N_i kT/h \exp((-\Delta Fg(T)+\Delta F_{\mathrm{act}}(T))/kT). \qquad (3)$$

In this equation N_i is the number of molecules in the liquid per cm^3, h is the Planck constant, k is the Boltzmann constant, and T the absolute temperature. ΔFg is the formation energy of the critical nucleus and ΔF_{act} is the activation energy related to the barrier for water molecules binding to a water cluster. Using the activation energies given by Pruppacher[27] and our measured nucleation rates, we can calculate ΔFg, the energy of formation of the critical nucleus (Fig. 12). It decreases linearly with decreasing temperature by 8.5 $\mathrm{kJ\,mol^{-1}\,K^{-1}}$. In the same temperature range the activation energy ΔF_{act} as given by Pruppacher drops from 32.6 to 31.8 kJ/mol.[27] Thus the observed strong temperature dependence of the nucleation rate is mainly due to the temperature dependence of ΔFg, which as an extensive quantity depends strongly on the size of the critical nucleus. According to

$$\Delta Fg=\sigma_{i/w}\tfrac{4}{3}\pi r_i^2, \qquad (4)$$

the radius r_i of the critical nucleus may be calculated, if the interfacial energy $\sigma_{i/w}$ is known. For the calculations we used the $\sigma_{i/w}$ values tabulated by Pruppacher[1] and arrive at a temperature dependent size of the critical nucleus which radius ranges from 1.4 nm at $T=236.1\,\mathrm{K}$ and 1.5 nm at $T=237.3\,\mathrm{K}$. Under the same conditions Pruppacher[1] obtained slightly larger values of 1.1 to 1.2 nm which result from the difference in the nucleation rates as discussed above.

The observed scattering patterns and the measured depolarization rates of the frozen droplets suggest that polycrystalline ice particles are formed after freezing. Under our experimental conditions they tend to assume a spherical overall shape.

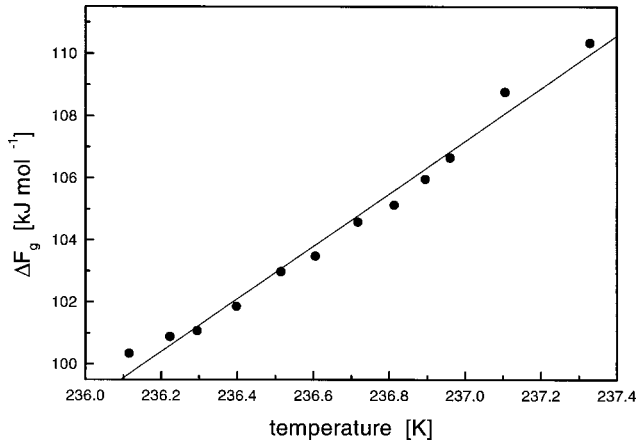

FIG. 12. Temperature dependence of the formation energy ΔFg of the critical nucleus based on the experimental results.

Understanding the phase behavior and phase transitions of supercooled water on a molecular level is still an interesting and open question as documented by recent publications on the thermodynamics of supercooled water[44–46] and by many theoretical works, mainly MD (molecular dynamics) calculations.[47,48] Many efforts have been devoted to understand the dynamics of the hydrogen bond network in liquid water, which is randomly percolated through space.[49] Individual water molecules are embedded in the network and cannot move independently but should move collectively. The formation of critical nuclei is, therefore, strongly connected with the growth and collapse of structural patterns in that hydrogen bond network. In order to correlate the nucleation rates with the structure of liquid water it is necessary to know how many water molecules are involved in the collective motions and how these motions are correlated in space and time. This question cannot be directly addressed by our experiment, but our results provide precise and reliable nucleation rates to test the validity of the various theoretical models.

CONCLUSION

We have measured rates for the homogeneous freezing of single water droplets inside an electrodynamic particle trap as a function of the particle temperature and charge. The combination of accurate droplet size determination with a statistical analysis of the freezing process of several thousand droplets allowed to obtain much more precise rates than previously available. Such accurate measurements yield not only important input parameters for atmospheric modeling, but may in future help to improve the still semiempirical microscopic theories of the liquid–solid phase transition.

ACKNOWLEDGMENTS

Financial support by the Kommission für Forschung und Nachwuchs of the Freie Universität Berlin is gratefully acknowledged.

[1] H. Pruppacher and J. D. Klett, *Microphysics of Clouds and Precipitation*, 2nd ed. (Kluwer, Dordrecht, 1998).
[2] M. Del Guasta, M. Morandi, L. Stefanutti, S. Balestri, E. Kyrö, M. Rummukainen, V. Rizi, V. Rizi, B. Stein, C. Wedekind, B. Mielke, R. Matthey, V. Mitev, and M. Douard, J. Aerosol Sci. **29**, 357 (1998).
[3] M. Volmer and A. Weber, Z. Phys. Chem. (Leipzig) **119**, 277 (1925).
[4] L. Farkas, Z. Phys. Chem. **A 125**, 236 (1927).
[5] R. Becker and W. Döring, Ann. Phys. (Leipzig) **24**, 719 (1935).
[6] J. Frenkel, J. Chem. Phys. **7**, 538 (1939).
[7] M. Volmer, *Kinetik der Phasenbildung* (Steinkopff, Dresden, 1939).
[8] J. Zeldovich, Zh. Eksp. Teor. Fiz. **12**, 525 (1942).
[9] D. Turnbull and J. C. Fisher, J. Chem. Phys. **17**, 71 (1949).
[10] F. J. Farley, Proc. R. Soc. London, Ser. A **212**, 530 (1952).
[11] J. Frenkel, *Kinetic Theory of Liquids* (Dover, New York, 1955).
[12] J. D. Bernal and R. H. Fowler, J. Chem. Phys. **1**, 515 (1933).
[13] Y. U. V. Gurikov, Zh. Strukt. Khim. **1**, 286 (1960); **6**, 817 (1965).
[14] H. S. Frank and A. S. Quist, J. Chem. Phys. **34**, 604 (1961).
[15] H. S. Frank and W. Y. Wen, Discuss. Faraday Soc. **24**, 135 (1957).
[16] G. Nemethy and H. A. Scheraga, J. Chem. Phys. **36**, 3382 (1962); **41**, 680 (1964).
[17] G. Nemethy and H. A. Scheraga, J. Phys. Chem. **77**, 3092 (1973).
[18] C. A. Angell, Annu. Rev. Phys. Chem. **34**, 593 (1983).
[19] G. T. Butorin and V. P. Skripov, Kristallografiya **17**, 379 (1972).
[20] D. E. Hagen, R. J. Anderson, and J. L. Kassner, Jr., J. Atmos. Sci. **38**, 1236 (1981).
[21] R. J. Anderson, R. C. Miller, J. L. Kassner, Jr., and D. E. Hagen, J. Atmos. Sci. **37**, 2508 (1980).
[22] P. J. DeMott and D. C. Rogers, J. Atmos. Sci. **47**, 1056 (1990).
[23] P. Taborek, Phys. Rev. B **32**, 5902 (1995).
[24] K. Sassen and G. C. Dodd, J. Atmos. Sci. **45**, 1357 (1988).
[25] A. J. Heymsfield and R. M. Sabin, J. Atmos. Sci. **46**, 2252 (1989).
[26] A. J. Heymsfield and L. M. Miloshevich, J. Atmos. Sci. **50**, 2335 (1993).
[27] H. R. Pruppacher, J. Atmos. Sci. **52**, 1924 (1995).
[28] C. A. Jeffery and P. H. Austin, J. Geophys. Res. **102**, 25269 (1997).
[29] B. Krämer, M. Schwell, O. Hübner, H. Vortisch, T. Leisner, E. Rühl, H. Baumgärtel, and L. Wöste, Ber. Bunsenges. Phys. Chem. **100**, 1911 (1996).
[30] W. Paul and H. Steinwedel, Z. Naturforsch. A **8**, 448 (1953).
[31] R. F. Wuerker, H. Shelton, and R. V. Langmuir, J. Appl. Phys. **30**, 342 (1959).
[32] E. J. Davis, Aerosol. Sci. Technol. **26**, 212 (1997).
[33] D. G. Imre, J. Xu, and A. C. Tridico, Geophys. Res. Lett. **24**, 69 (1997).
[34] K. L. Carleton, D. M. Sonnenfroh, W. T. Rawlins, B. E. Wyslouzil, and S. Arnold, J. Geophys. Res. **102**, 6025 (1997).
[35] G. L. Switzer, Rev. Sci. Instrum. **62**, 2765 (1991).
[36] Microdrop Gesellschaft für Mikrodosiersysteme mbH, Mühlenweg 143, 22844 Norderstedt, Germany
[37] M. D. Barnes, N. Lermer, W. B. Whitten, and J. M. Ramsey 2287.
[38] B. Steiner, B. Berge, R. Gausmann, J. Rohmann, E. Rühl, Appl. Opt. **38**, 1523 (1999).
[39] C. F. Bohren and D. R. Huffmann, *Absorption and Scattering of Light by Small Particles* (Wiley, New York, 1983).
[40] H. R. Pruppacher, J. Chem. Phys. **39**, 1586 (1963).
[41] T. Koop, B. Luo, U. M. Biermann, P. J. Crutzen, and T. Peter, J. Phys. Chem. **101**, 1117 (1997).
[42] B. Stein, C. Wedekind, H. Wille, F. Immler, M. Müller, L. Wöste, M. del Guasta, L. Stefanutti, V. Rizzi, G. Readelli, V. Mitev, R. Matthey, R. Kivi, and E. Kyrö, J. Geophys. Res. (in press).
[43] M. Del Guasta, M. Morandi, L. Stefanutti, B. Stein, J. Kolenda, P. Rairoux, J. P. Wolf, R. Matthey, and E. Kyro, Geophys. Res. Lett. **21**, 1339 (1994).
[44] P. G. Debendetti, *Metastable Liquids, Concepts and Principles* (Princeton University Press, Princeton, N.Y., 1996).
[45] L. P. N. Rebelo, P. G. Debenedetti, and S. Sastry, J. Chem. Phys. **109**, 626 (1998).
[46] C. A. Jeffery and P. H. Austin, J. Chem. Phys. **110**, 484 (1999).
[47] D. Marx, M. E. Tuckermann, J. Hutter, and M. Parinello, Nature (London) **397**, 601 (1999).
[48] F. Sciortino, A. Geiger, and H. E. Stanley, J. Chem. Phys. **96**, 3857 (1992).
[49] A. Geiger, F. H. Stillinger, and A. Rahman, J. Chem. Phys. **70**, 4185 (1979).